KCu_7P_3: A Two-Dimensional Noncentrosymmetric Metallic Pnictide

Alexander J. E. Rettie[1], Christos D. Malliakas[2], Antia S. Botana[3], Jin-Ke Bao[1], Duck Young Chung[1], Mercouri G. Kanatzidis[1,2,*]

1. Materials Science Division, Argonne National Laboratory, Argonne, IL, 60439, USA
2. Department of Chemistry, Northwestern University, Evanston, IL, 60208, USA
3. Department of Physics, Arizona State University, Tempe, AZ, 85281, USA

Layered material, flux synthesis, p-type metal, aqueous stability

ABSTRACT: We report a 2D material, KCu_7P_3 with a noncentrosymmetric structure (trigonal space group $P31m$, a = 6.9637(2) Å, c = 24.1338(10) Å), which forms both from a molten potassium polyphosphide flux and from the elements. This phase consists of infinite $[Cu_7P_3]^-$ layers with hexagonal P sheets separated by K^+ ions. The structure of the layers is unique but related to both Cu_3P and the $CaCu_4P_2$ structure-types. Single-crystal refinement reveals extensive disorder within the Cu_3P-like slabs. KCu_7P_3 is paramagnetic and exhibits a room temperature resistivity of ~335 μΩ-cm with a metal-like temperature dependence. The metallic character is supported by density functional theory electronic structure calculations. Hall and Seebeck effect measurements yield *p*-type behavior with a hole mobility of ~15 $cm^2\ V^{-1}\ s^{-1}$ at 300 K and a carrier concentration on the order of $10^{21}\ cm^{-3}$. KCu_7P_3 is chemically stable in ambient conditions, as well as aqueous neutral and acidic solutions.

INTRODUCTION

The copper pnictides are rich both in structural diversity[1-3] and functional properties. The binary Cu_3P for example, shows promise as an anode material for Li-ion batteries[4] and as a bifunctional electrocatalyst for the hydrogen and oxygen evolution reactions.[5-7] Cu ions in these compounds often exhibit static or dynamic disorder, which can render them prone to electronic and structural instabilities. The dimensionality and electronic structure of these compounds may be modified *via* the introduction of alkali or alkaline earth cations. Copper-pnictide motifs range from the 0D molecular units in K_5CuPn_2 (*Pn* = As, Sb),[8-10] 1D chains in A_2CuPn (A = Na, K; *Pn* = P, As, Sb),[11-12] 2D layers observed in $(A/AE)Cu_4Pn_2$ (*A*/*AE* = Na, K, Ca-Ba; *Pn* = P, As, Sb)[13-15] and 3D networks as found in $BaCu_8Pn_2$ (*Pn* = P, As).[16]

Flux synthesis is a powerful route to new materials, often yielding metastable phases.[17-18] A case in point is the use of alkali metal chalcogenides as reactive fluxes, which has enabled the synthesis of a multitude of compounds.[19-23] These polychalcogenides are ideal for this purpose due to their moderate melting points and numerous congruently melting phases.[24-25] By contrast, alkali metal pnictides (especially phosphides) are relatively unexplored as reactive fluxes. Indeed, in the K-P phase space only K_3P_7 is reported to melt congruently at 930 °C,[26-27] with all other known phases decomposing at elevated temperatures. In the K-Cu-P phase space only $K_3Cu_3P_2$[28] and K_2CuP[11] have been reported, suggesting it is ripe for exploration.

Here, we report the synthesis of KCu_7P_3 from a potassium polyphosphide flux. The compound is 2D and features Cu_3P-like slabs separated by K^+ ions. The crystallographic structure solution was non-trivial because of plate-like crystal morphology, crystal twinning and Cu^+ ion disorder present in the structure. Charge transport experiments and supporting electronic structure calculations show that the new compound is a *p*-type metal. KCu_7P_3 is stable in air as well as in neutral and acidic aqueous media. To the best of our knowledge, this is the first synthesis report using a molten alkali metal polyphosphide as a reactive flux.

EXPERIMENTAL SECTION

Reagents. Potassium metal (99%, Sigma-Aldrich) and red phosphorous powder (99%, Beantown Chemical) were used without further modification. Copper powder (99.9%, Sigma-Aldrich) was washed with concentrated acetic acid to remove a native oxide layer, evidenced by a color change from red/orange to pale pink. The washed Cu powder was dried and stored in an Argon-filled glovebox.

Synthesis. Synthetic operations were carried out under an Argon atmosphere in an M-Braun glovebox (O_2 and H_2O concentrations < 0.1 ppm). The synthesis of alkali metal phosphides is non-trivial and caution should be used during handling and disposal.[1, 29] The K_3P_7 flux was synthesized using a vapor transport technique.[18] First, K metal pieces (0.663 g, 16.96 mmol) were first loaded into an 18 mm o.d. × 16 mm i.d. fused-silica tube. Subsequently, an alumina crucible containing red P (1.167 g, 37.68 mmol) was placed above the metal chunks before flame-sealing under vacuum (< 10^{-4} mbar). A small excess of K metal (5% molar) was used. This assembly was placed vertically in a muffle furnace, heated to 500 °C in 12 hrs and soaked for 12 hrs before the furnace was turned off. A visually inhomogeneous

K_3P_7 powder could be collected from the crucible and was homogenized before further use. During flux synthesis, K_3P_7 (0.918 g, 2.75 mmol) and Cu (0.082 g, 1.29 mmol) were homogenized using a mortar and pestle, loaded into an Al_2O_3 crucible and capped with another Al_2O_3 crucible in an Nb can. This can was then welded shut under an Ar atmosphere and flame-sealed in an evacuated 18 mm o.d. × 16 mm i.d. fused-silica jacket to prevent oxidation. The reaction vessel was heated to 1030 °C in 12 hrs and held for 12 hrs before cooling to 700 °C at 2 °C min^{-1} after which the furnace was turned off. The resultant black ingot was washed in ethanol under flowing N_2 to remove unreacted flux. Soft, plate-like crystals with metallic appearance were finally rinsed with ethyl ether and dried (see Figure S1 in the Supporting Information (SI)).

Phase-pure powder was synthesized directly from the elements using a multi-step heating profile to mitigate the exothermic reaction of K and P. Cu and red P powder were ground together before K pieces were rolled in the mixture and placed on top of the powder in an Al_2O_3 crucible. This assembly was then capped with a second alumina crucible and sealed in a 15 mm o.d. × 13 mm i.d. evacuated fused-silica tube. The sealed ampule was first heated slowly to 300 °C in 30 hrs, soaked for 6 hrs and then heated to 500 °C in 12 hrs where it was held for 12 hrs before the furnace was turned off. This visually inhomogeneous mixture was re-homogenized in an Ar glovebox and further reacted at 500 °C for 12 hrs in an identical assembly. Several elemental ratios were trialed, with K:Cu:P ratios of 1:4:2 and 1:5.5:2.5 producing phase-pure material by PXRD (Figure S2 in the SI). These products were thoroughly washed with ethanol under flowing N_2 and then water. Polycrystalline pellets were produced by cold-pressing the washed powders in a die, resulting in compacts with >80% theoretical density. Annealing treatments in vacuum at 300 and 500 °C for 12 hrs were attempted to increase density but resulted in decomposition by PXRD and no significant mass or volume change.

Single-Crystal X-ray Diffraction. A thin crystal plate was selected and fixed on a glass fiber for X-ray diffraction at room temperature. Intensity data were collected using ω scans on a Bruker-APEX II CCD diffraction system with microfocused Mo Kα radiation (λ = 0.71073 Å). Single frames were collected using a 3 min exposure time and ω rotation angle of 0.5°. Data integration and multi-scan absorption corrections were performed using Bruker SAINT (version 8.38a) and SADABS software packages respectively. SHELXL[30], OLEX2[31] and JANA2006[32] software packages were used to solve and refine the crystal structure. Details of data collection and the structural refinement are located in Table 1. Atomic coordinates, thermal displacement parameters (U_{eq}), and occupancies of all atoms can be found in Table S2 in the Supporting Information. Anisotropic displacement parameters (ADPs) are given in Table S3. Tables S4 and S5 contain selected bond lengths and angles respectively.

Powder X-ray Diffraction. Powder X-ray diffraction (PXRD) was used to assess phase purity using a Rigaku Miniflex diffractometer with a Ni-filtered Cu Kα source (15 mA and 40 kV). Continuous scanning and spinning were utilized with a step size of 0.015°. Finely-ground powders were dispersed on a flat sample holder or crystal plates were pressed flat on the holder with a glass slide to check orientation and phase.

Synchrotron X-ray Diffraction. Synchrotron XRD data were measured at beamline 11-BM at the Advanced Photon Source (APS) at Argonne National Laboratory. Undiluted KCu_7P_3 powder was sieved to < 40 μm and placed in a Kapton capillary (0.5 mm O.D.) which was mounted to a magnetic sample holder. Samples were spun during collection and the X-ray wavelength was 0.41275 Å. Refinements were performed using GSAS-II software,[33] using the structural model from single-crystal refinement as a starting point.

Scanning Electron Microscopy. Crystal composition and appearance were determined using a S-4700-II scanning electron microscope (SEM, Hitachi) with an energy-dispersive X-ray spectrometer (EDS). The spectrometer utilizes an XFlash 6|60 detector (Bruker), and a beam current of 20 μA at 15 kV accelerating voltage was used for data collection.

Charge Transport Properties. Temperature-dependent resistivity and Hall effect measurements on plate-like crystals (approximate dimensions: 1 × 1 × 0.03 mm^3) were performed on a Dynacool Physical Property Measurement System (PPMS, Quantum Design) from 1.8 to 300 K. Resistivity measurements employed a 4-point collinear geometry and two voltage contacts were placed perpendicular to the axis of current flow in the sample plane for Hall effect measurements. Both measurements were performed concurrently on the same sample in all cases. A magnetic field from -9 to +9 T was applied perpendicular to the sample plane. Data reproducibility was confirmed by repeated temperature and field cycling. Silver paste (DuPont), colloidal graphite paste (Ted Pella) and sputtered Pt contacts were all found to produce stable, Ohmic contact to KCu_7P_3. Seebeck coefficient measurements were made on a pressed polycrystalline pellet about 1 mm thick using the thermal transport option (TTO) in the symmetrical configuration Cu|Ag paste|KCu_7P_3|Ag paste|Cu.

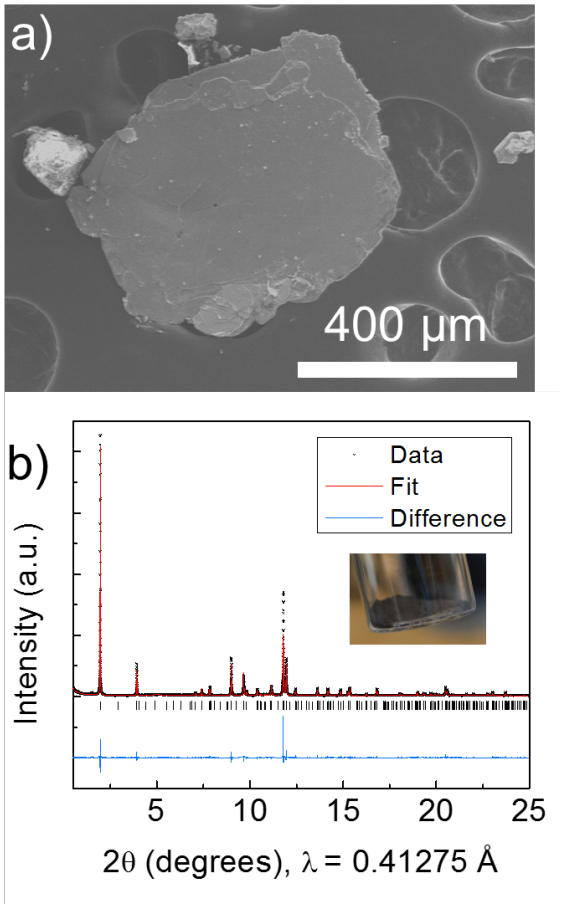

Figure 1. a) SEM image of a KCu_7P_3 crystal illustrating a plate-like morphology. **b)** Rietveld refinement of KCu_7P_3 powder synthesized from the elements and washed with ethanol and water. High-resolution synchrotron XRD data were collected at 298 K. Vertical lines indicate the positions of reflections. Inset: photograph of dark grey KCu_7P_3 powder in a 27.5 mm diameter glass vial.

Electronic Structure Calculations. Density functional theory (DFT)-based calculations were performed with the all-electron, full potential code WIEN2k[34] based on the augmented plane wave plus local orbitals (APW+lo) basis set.[35] The exchange correlation functional chosen to study KCu_7P_3 was the Perdew-Burke-Ernzerhof of the generalized gradient approximation (GGA).[36] $R_{mt}K_{max}$= 7.0, was used for our calculations. The chosen muffin-tin radii were 2.5, 2.29 and 1.89 a.u. for K, Cu and P, respectively. For the purposes of these calculations, the split site in the crystal structure used to model Cu disorder were represented by a single non-split Cu atom.

The transport properties were calculated using Boltzmann transport theory within the constant scattering-time approximation as implemented in the BoltzTrap code.[37] A very dense 34 × 34 × 8 k mesh was required to obtain convergence. Within this approach the Seebeck coefficient has no dependence on τ.

Magnetic Properties. Magnetic moment versus temperature of a KCu_7P_3 powder compact (mass = 29.4 mg) in a plastic holder was measured in a MPMS (Quantum Design). Data were converted into molar susceptibility per Cu atom, X_m and fit using a modified Curie-Weiss equation:

$$X_m(T) = X_{TIP} + C/(T-\theta) \qquad (1)$$

where, T is temperature, X_{TIP} is the temperature-independent susceptibility, C is the Curie constant and θ is the Curie-

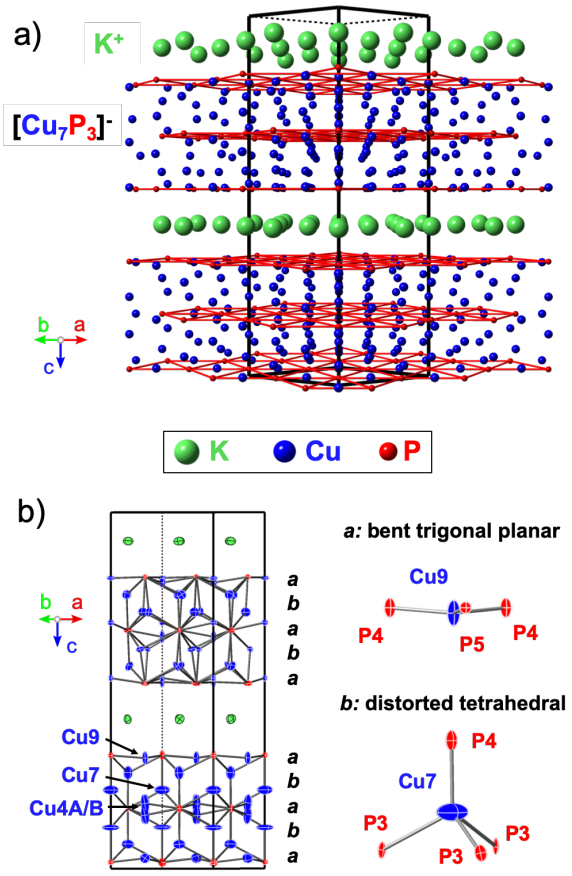

Figure 2. a) Crystal structure of KCu_7P_3 showing hexagonal phosphorous sheets that comprise the $[Cu_7P_3]^-$ blocks in red. **b)** Left: structure showing anisotropic displacement parameters. Right: detailed view of the Cu-P coordination using atoms Cu7 and Cu9. Thermal ellipsoids are set at 75%. The trigonal unit cell is shown with black lines.

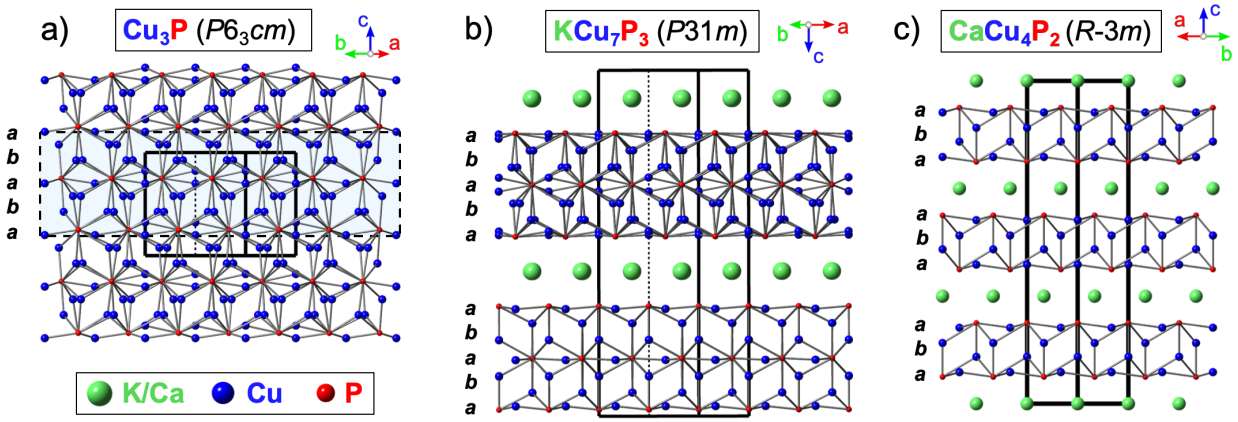

Figure 3. Structural relationships between Cu-P networks in room temperature **a)** Cu_3P, **b)** KCu_7P_3 and **c)** $CaCu_4P_2$. The *ababa* stacking sequence refers to layers of distorted trigonal planar (*a*) and distorted tetrahedral (*b*) Cu atoms that comprise the Cu-P blocks (illustrated in Figure 2b). The Cu_3P area highlighted in blue with dashed lines in **a)** resembles the structure of the $[Cu_7P_3]^-$ layers shown in **b)**. The unit cells are shown with solid black lines.

Weiss temperature. The effective moment of Cu in Bohr magnetons was determined using the relationship for cgs units, $\mu_{eff} = 2.827\sqrt{C}$.[38]

Stability in Aqueous Solutions. Approximately 100 mg of KCu_7P_3 powder was dispersed in ~20 mL of unbuffered deionized water, 1 M NaOH or 0.05 M H_2SO_4 and was soaked in these solutions for 12 hrs with occasional agitation. The powder was then filtered and washed copiously with water before drying at room temperature under vacuum.

RESULTS AND DISCUSSION

Synthesis. KCu_7P_3 was initially obtained as the major product of the reaction of K_3P_7 flux with Cu metal (~2.1:1 molar ratio) at 1030 °C. Crystals were harvested by repeated washing with ethanol under flowing N_2 and their approximate composition was measured by EDS before structure solution using single-crystal XRD. The crystals were thin (< 50 μm), mechanically soft and stable in ambient conditions. A layered morphology was evident from SEM (Figure 1a) and compositional analysis by EDS yielded the stoichiometry: $K_{1.00(3)}Cu_{7.2(2)}P_{2.9(1)}$.

Phase-pure polycrystalline powder was produced from the elements using a multi-stage heating profile and a second annealing step with intermediate grinding to achieve a homogenous product. Interestingly, phase-pure material by PXRD was only achieved in synthesis conditions where K and P were in excess (Figure S2 in the SI). These powders would react with ethanol (briefly producing bubbles), or violently with water, presumably due to the presence of an amorphous and highly reactive K-P byproduct. Therefore, the powders were washed with ethanol under flowing N_2 and then water before physical property measurements. Unit cell parameters obtained *via* Rietveld refinement (R = 8.0%, wR = 10.7%, χ^2 = 3.4) of synchrotron XRD data (Figure 1b) were in good agreement with those from single-crystal XRD (a = 6.9646(1) Å, c = 24.1501(4) Å, Z = 6, V = 1014.49(4) Å^3). Further details of the Rietveld refinement are available in the SI. Annealing experiments on pressed pellets under vacuum at 300 °C for 12 hrs showed a minor amount of Cu_3P by PXRD after heat treatment (see Figure S3 in the SI). Thus, KCu_7P_3 is a metastable phase, decomposing below 300 °C.

Crystal Structure. Room temperature single-crystal XRD was used to determine the crystal structure of KCu_7P_3. The plate-like crystals had a metallic sheen and only very small samples (~50 × 50 × 10 μm) produced suitable datasets for structure solution. These were picked from the reaction product and not cut or broken from larger samples. It crystallizes in a new structure-type with the noncentrosymmetric (NCS) trigonal space group $P31m$ (No. 157), a = 6.9637(2) Å, c = 24.1338(10) Å, Z = 6 and V = 1013.53(7) Å^3. $P31m$ is one of the 10 NCS polar crystal classes, $3m$ (C_{3v}), with the polar axis being the c-axis.[39] Crystallographic information is contained in Tables 1 and S2-S5 in the SI.

KCu_7P_3 consists of infinite $[Cu_7P_3]^-$ layers separated by K^+ ions (Figure 2a). Each layer contains three hexagonal sheets of P atoms ~4.3 Å apart. In between these Cu ions reside in either bent trigonal planar (*a*) or distorted tetrahedral (*b*) environments with P. Within the slabs, the two Cu-P environments are also arranged in layers forming an *ababa* stacking sequence (Figure 2b). The Cu-P and Cu-Cu bond lengths of ~2.3-2.7 Å and ~2.5 Å respectively, are in good agreement with the related compounds Cu_3P and $CaCu_4P_2$. The two unique K^+ ions that separate the layers are six-fold coordinated with P in slightly distorted octahedral environments.

The crystallographic structure solution was non-trivial due to the small size and plate-like morphology of suitable crystals, in addition to twinning and disorder present in the structure. All datasets contained a 4-fold twin with 50% fraction. Large anisotropic displacement parameters (ADPs) were observed for the

Cu atoms, indicative of static or dynamic disorder (Tables S2 and S3). This is common in Cu-containing materials, *e.g.*, $Cu_{3-x}P$,[40] $CaCu_4P_2$,[14] $KCu_{3-x}Se_2$[41] and $NaCu_4Se_3$.[42] Significant disorder of both Cu and P atoms was further evidenced by the need to invoke site splitting of Cu4 (Figure 2b) and the addition of EADP and ISOR constraints to obtain physical values for the ADPs of these species. The crystallographic information file is provided in the Supporting Information (KCu7P3_300K.cif). During refinement a higher symmetry space group was initially suggested ($P6_3cm$) but resulted in large R values (> 30%). It was necessary to lower the symmetry to $P31m$ – decoupling the layers – to solve the structure.

The structure of KCu_7P_3 can be described as a dimensionally-reduced derivative of the binary compound Cu_3P which shares a trigonal polar space group and nearly identical a lattice parameter ($P6_3cm$, a = 6.9593(5) Å, c = 7.143(1) Å).[43] Inspection of the room temperature Cu_3P structure shows that 2D $[Cu_7P_3]^-$ slabs can be excised directly from the 3D parent compound (Figures 3a and b). The NCS character derives from geometric displacements of some Cu ions (Cu(12), Cu(14), Cu(16) and Cu(17)) in the top slab, closely resembling NCS Cu_3P.

The bottom $[Cu_7P_3]^-$ slab does not share these geometric displacements, with all Cu atoms sitting on (n/3, m/3, z) positions, where n and m are integer values. This Cu atom geometry is similar to that in the $[Cu_4P_2]^{2-}$ layers of the $CaCu_4P_2$ structure-type, which crystallizes in the centrosymmetric space group R-3m (Figure 3c).[14] Although we did not observe any KCu_4P_2 in our experiments (see Figure S2 in the SI), ACu_4Pn_2 (A = Na, K; Pn = As, Sb)[13] have been reported in addition to alkali earth analogues.[15] Therefore, ACu_7Pn_3 may be part of a large family of dimensionally-related compounds:

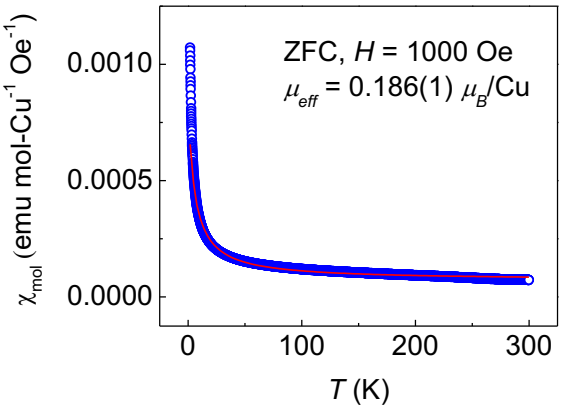

Figure 4. Zero-field cooled (ZFC) molar magnetic susceptibility from 1.8-300 K under an applied field of 1000 Oe (open symbols). The data were fit to a modified Curie-Weiss law (red solid line) yielding an effective moment of 0.186(1) μ_B/Cu.

$([A/AE]_xPn)_m(Cu_3Pn)_n$, where doping can be easily achieved by elemental substitution on the A/AE site.[44-45]

Magnetic Properties. In order to determine the oxidation state of Cu, the molar magnetic susceptibility of KCu_7P_3 powder was measured from 1.8 to 300 K (Figure 4). The compound showed paramagnetic behavior, which was fit to a modified Curie-Weiss law (Equation 1) yielding χ_{TIP} = 7.14(2)×10^{-5} emu mol-Cu^{-1} Oe^{-1}, C = 4.34(3)×10^{-3} emu K mol-Cu^{-1}, θ = -5.6(1) K and a small effective moment, μ_{eff} of 0.186(1) μ_B/Cu. As this value is considerably smaller than the theoretical μ_{eff} for Cu^{2+} of 1.73 (spin 1/2), the magnetic properties of KCu_7P_3 are consistent with Cu primarily being in the 1+ oxidation state and the sample containing paramagnetic impurities. This has also been observed in the compounds $NaCu_4Se_3$ and $NaCu_6Se_4$.[42, 46] Considering strict integer valence arguments, this would imply mixed-valence falling on the phosphorous atoms in the structure, *e.g.*, $K^+(Cu^+)_7(P^{3-})_2P^{2-}$. However, because there is no P-P bonding within the layers, we propose that KCu_7P_3 is best thought of as Cu_3P intercalated with K^+ ions that hole-dope the $[Cu_7P_3]^-$ slabs. As we will discuss later, the holes are delocalized due to high covalent Cu-P bonding, resulting in a Cu valence state slightly greater than 1+, a P valence slightly less than

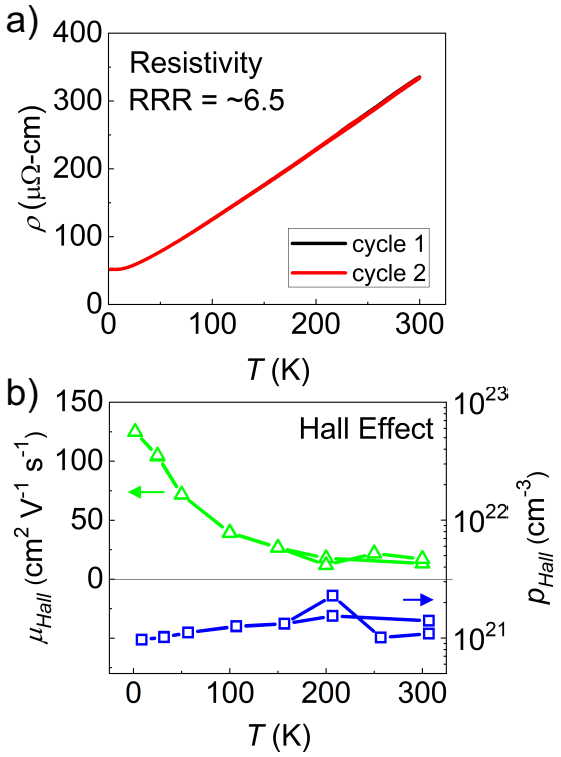

Figure 5. a) Resistivity and **b)** Hall effect of a KCu_7P_3 crystal from 1.8 to 300 K. The residual resistivity ratio (RRR = ρ(300 K)/ρ(1.8 K)) was ~6.5. Data from both cooling and warming are shown.

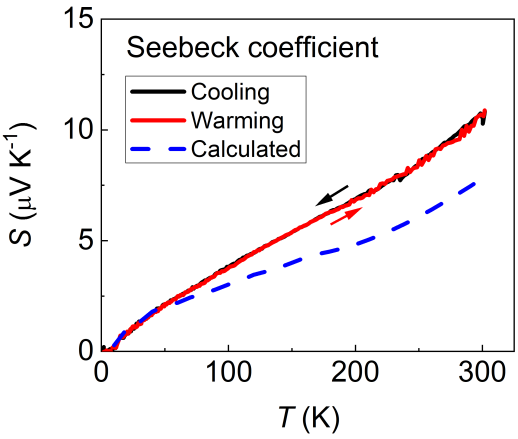

Figure 6. Seebeck coefficient of a pressed polycrystalline pellet of KCu_7P_3. Experimental data is shown with solid lines and compared to the calculated Seebeck coefficient using Boltzmann transport theory (dashed line).

3– and metallic behavior.

Charge Transport. Temperature-dependent resistivity measurements show that KCu_7P_3 has a low room temperature resistivity ~335 μΩ-cm with a metallic temperature dependence (Figure 5a). The residual resistivity ratio (RRR = ρ(300 K)/ρ(1.8 K)) was ~6.5, indicating moderate crystal quality possibly due to defects and twinning in the samples. Current flow was approximately in-plane for all measurements. Hall effect experiments yielded linear Hall resistances with magnetic field, thus the equation for a single parabolic band was used.[47] Holes were the majority carriers and a large carrier concentration, p_{Hall}, on the order of 10^{21} cm^{-3} was measured, corresponding to moderate hole mobility of ~15 cm^2 V^{-1} s^{-1} at room temperature. With decreasing temperature, p_{Hall} was effectively constant, while the hole mobility rose to ~150 cm^2 V^{-1} s^{-1} at 1.8 K. The transverse magnetoresistance was positive and reached a maximum at 1.8 K and 9 T of ~17% (Figure S4 in the SI). Similar transport behavior was measured on a second crystal and these data are located in the SI (Figure S5). Seebeck coefficient measurements on a polycrystalline sample yielded a value that was small and positive (Figure 6). Taken with the large, temperature-invariant carrier concentration from Hall effect measurements, we assign KCu_7P_3 as a *p*-type metal. The experimental Seebeck data compare well to those calculated from the electronic band structure using Boltzmann transport theory (dashed line in Figure 6), to be discussed below.

Band Structure Calculations. The calculated electronic band structure and density of states indicate metallic behavior for KCu_7P_3 (Figure 7a). Around the Fermi level (E_F), Cu 3d states dominate with a significant contribution from P 3p states, consistent with highly covalent Cu-P bonding within the layers. The Fermi surface is complex with numerous band crossings, yielding a hole carrier concentration of ~3×20^{21} cm^{-3}. Of note are several band crossings at the K and H points of the Brillouin zone, which manifest as a spike in the density of states at E_F. The Brillouin zone used in the calculations can be located in the SI (Figure S6).

Our transport and structural characterizations show KCu_7P_3 is both a metal and has a NCS crystal structure. NCS metals often exhibit anisotropic Seebeck coefficients and have potential applications as ultrafast thermal radiation detectors.[48-50] Therefore, future work will focus on measuring the Seebeck coefficient along the principal axes using KCu_7P_3 single crystals. $Cu_{3-x}P$ also has a NCS structure and has been assigned as a *p*-type metal based on resistivity[51-52] and Hall effect[40] measurements. However, we note that a degenerately-doped semiconductor with a small band gap would yield similar results. This situation would be expected as stoichiometric Cu_3P is valence-precise and should exhibit semiconducting behavior. Seebeck coefficient measurements and band structure calculations would be valuable in clarifying the electronic nature of $Cu_{3-x}P$ and hence, its relationship to KCu_7P_3 and related phases.

Stability in Aqueous Solutions. Tests in aqueous solutions indicated that KCu_7P_3 is stable after prolonged soaking in unbuffered water and 0.05 M H_2SO_4 (*aq*) but degraded slightly in basic media (Figure 8). The only other reported phases in the K-Cu-P phase space ($K_3Cu_3P_2$[28] and K_2CuP[11]) are K-rich and decompose rapidly in moist air. We note that $CaCu_4P_2$ is reported as stable in ambient conditions also,[14] meaning these dimensionally reduced, Cu-rich Cu_3P derivatives may be of interest for applications in aqueous solutions, *e.g.*, electrocatalysis.

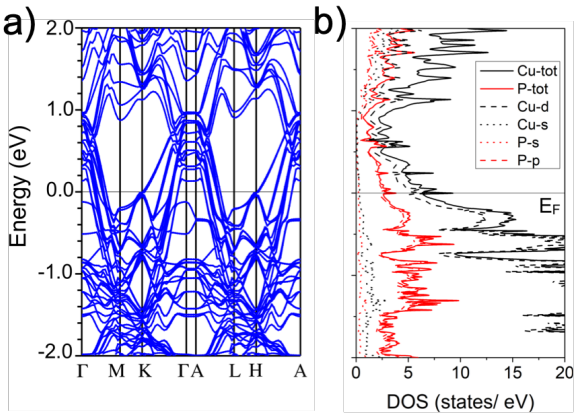

Figure 7. a) Electronic band structure along high symmetry directions (see Figure S6) and **b)** orbital-projected density of states plots for hexagonal KCu_7P_3. The Fermi level (E_F) is set at 0 eV.

CONCLUSIONS

The new 2D noncentrosymmetric pnictide, KCu_7P_3 was discovered from a molten potassium polyphosphide flux and subsequently synthesized directly from the elements. It crystallizes in the polar *P*31*m* space group, consisting of $[Cu_7P_3]^-$ slabs with a disordered Cu sublattice and hexagonal P sheets. The spaces between these slabs host the charge balancing K^+ ions. Although

KCu_7P_3 is thermally metastable and decomposes on heating, the phase is stable in ambient conditions as well as neutral and strongly acidic solutions. Resistivity, Hall and Seebeck effect measurements are consistent with KCu_7P_3 being a *p*-type metal, with $p_{Hall} = \sim 10^{21}$ cm^{-3} and $\mu_{Hall} = \sim 15$ cm^2 V^{-1} s^{-1} at room temperature. Band structure calculations support this description. Our work highlights that new materials may be discovered by using alkali metal polyphosphides as reactive fluxes in a similar fashion to the multitude of compounds synthesized using alkali metal polychalcogenide fluxes.

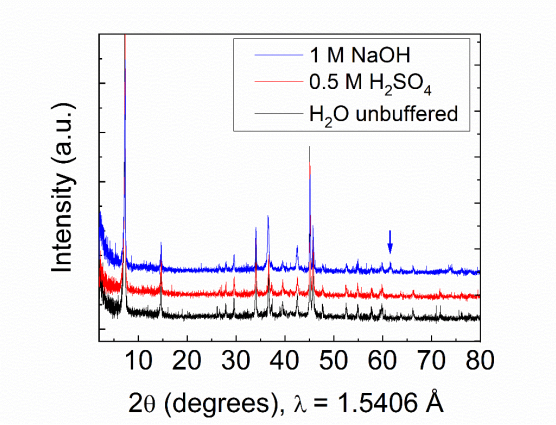

Figure 8. PXRD of KCu_7P_3 powder after being soaked in various aqueous solutions. A peak due to possible degradation after soaking in 1 M NaOH is indicated by an arrow.

ASSOCIATED CONTENT

Supporting Information

The Supporting Information is available free of charge on the ACS Publications website.

Details of synthesis, Rietveld refinement, additional transport, experimental and single-crystal refinement structural data.

AUTHOR INFORMATION

Corresponding Author

* m-kanatzidis@northwestern.edu

ACKNOWLEDGMENTS

This work was supported by the U.S. Department of Energy, Office of Science, Materials Sciences and Engineering Division. We gratefully acknowledge the computing resources provided on Blues, the high-performance computing clusters operated by the Laboratory Computing Resource Center at Argonne National Laboratory. The electron microscopy was accomplished at the Electron Microscopy Center for Materials Research at Argonne National Laboratory, a U.S. Department of Energy Office of Science Laboratory operated under Contract No. DE-AC02-06CH11357 by UChicago Argonne, LLC. We gratefully acknowledge Saul Lapidus for performing synchrotron XRD at Sector 11-BM. Single crystal X-ray work made use of the IMSERC at Northwestern University, which has received support from the Soft and Hybrid Nanotechnology Experimental (SHyNE) Resource (NSF ECCS-1542205); the State of Illinois and International Institute for Nanotechnology (IIN).

Table 1. Crystal data and structure refinement for KCu_7P_3 at 300 K.

Empirical formula	KCu_7P_3
Formula weight	576.79
Temperature	300 K
Wavelength	0.71073 Å
Crystal system	trigonal
Space group	*P* 3 1 *m* (No. 157)
Unit cell dimensions	a = 6.9637(2) Å, α = 90° c = 24.1338(10) Å, γ = 120°
Volume	1013.53(7) Å^3
Z	6
Density (calculated)	5.760 g/cm^3
Absorption coefficient	22.815 mm^{-1}
F(000)	1602
Crystal size	0.04 × 0.03 × 0.001 mm^3
θ range for data collection	0.848 to 34.441°
Index ranges	-10<=h<=10, -10<=k<=9, -38<=l<=37
Reflections collected	11960
Independent reflections	2937 [R_{int} = 0.0728]
Completeness to θ = 25.242°	99.4%
Refinement method	Full-matrix least-squares on F^2
Data / restraints / parameters	2937 / 19 / 133
Goodness-of-fit	1.082
Final R indices [I > 2σ(I)]	R_{obs} = 0.0638, wR_{obs} = 0.1787
R indices [all data]	R_{all} = 0.0879, wR_{all} = 0.1978
Largest diff. peak and hole	2.475 and -3.585 e·Å^{-3}

$R = \Sigma||F_o|-|F_c|| / \Sigma|F_o|$, $wR = (\Sigma[w(|F_o|^2 - |F_c|^2)^2] / \Sigma[w(|F_o|^4)])^{1/2}$ and $w=1/[\sigma^2(Fo^2)+(0.1022P)^2]$ where $P=(F_o^2+2F_c^2)/3$

REFERENCES

1. Von Schnering, H. G.; Hönle, W., Chemistry and structural chemistry of phosphides and polyphosphides. 48. Bridging chasms with polyphosphides. *Chem. Rev.* **1988,** *88* (1), 243-273.
2. Bawohl, M.; Nilges, T., Phosphorus rich d^{10} ion polyphosphides and selected materials. *Z. Anorg. Allg. Chem.* **2015,** *641* (2), 304-310.
3. Chen, J.-H.; Whitmire, K. H., A structural survey of the binary transition metal phosphides and arsenides of the d-block elements. *Coord. Chem. Rev.* **2018,** *355*, 271-327.
4. Pfeiffer, H.; Tancret, F.; Bichat, M.-P.; Monconduit, L.; Favier, F.; Brousse, T., Air stable copper phosphide (Cu_3P): a possible negative electrode material for lithium batteries. *Electrochem. Commun.* **2004,** *6* (3), 263-267.
5. Tian, J.; Liu, Q.; Cheng, N.; Asiri, A. M.; Sun, X., Self-Supported Cu_3P Nanowire Arrays as an Integrated High-Performance Three-Dimensional Cathode for Generating Hydrogen from Water. *Angew. Chem.* **2014,** *126* (36), 9731-9735.
6. Han, A.; Zhang, H.; Yuan, R.; Ji, H.; Du, P., Crystalline copper phosphide nanosheets as an efficient Janus catalyst for overall water splitting. *ACS Appl. Mater. Interfaces* **2017,** *9* (3), 2240-2248.
7. Hao, J.; Yang, W.; Huang, Z.; Zhang, C., Superhydrophilic and superaerophobic copper phosphide microsheets for efficient electrocatalytic hydrogen and oxygen evolution. *Adv. Mater. Interfaces* **2016,** *3* (16), 1600236.
8. Eisenmann, B.; Klein, J.; Somer, M., Linear anions $[CuAs_2]^{5-}$, $[AuP_2]^{5-}$ and $[AuAs_2]^{5-}$ in potassium compounds. *J. Alloys Compd.* **1992,** *178* (1-2), 431-439.
9. Savelsberg, G.; Schäfer, H., K_5CuSb_2–a Compound with Linear Sb-Cu-Sb-Units. *Z. Naturforsch. B* **1979,** *34* (6), 771-773.
10. Eisenmann, B.; Savelsberg, G.; Schäfer, H., Preparation and Crystal Structure of Na_2CuAs, K_2CuAs and K_2CuSb. *Z. Naturforsch. B* **1976,** *31* (10), 1344-1346.
11. Eisenmann, B.; Somer, M., On New Ternary Alkali Metal Phosphides: K_2CuP, NaZnP and K_4CdP_2. *Z. Naturforsch. B* **1985,** *40* (11), 1419-1423.
12. Savelsberg, G.; Schäfer, H., Preparation and Crystal Structure of Na_2CuP, K_2AgAs, K_2AgSb, and K_2AgBi. *Z. Naturforsch. B* **1977,** *32* (7), 745-748.
13. Weise, W.; Schuster, H. U., Ternary compounds of sodium and potassium with $CaCu_4P_2$-structure. *Z. Anorg. Allg. Chem.* **1986,** *535* (4), 143-147.
14. Mewis, A., Preparation and Crystal Structure of $CaCu_4P_2$. *Z. Naturforsch. B* **1980,** *35* (8), 942-945.
15. Dünner, J.; Mewis, A., Synthese und Kristallstruktur von ACu_4As_2 (*A*: Ca–Ba, Eu). *Z. Anorg. Allg. Chem.* **1999,** *625* (4), 625-628.
16. Pilchowski, I.; Mewis, A.; Wenzel, M.; Gruehn, R., $BaCu_8P_4$ and $BaCu_8As_4$: Preparation, Structure Determination, and Electron Microscopy Investigations. *Z. Anorg. Allg. Chem.* **1990,** *588* (1), 109-116.
17. Kanatzidis, M. G.; Pöttgen, R.; Jeitschko, W., The metal flux: a preparative tool for the exploration of intermetallic compounds. *Angew. Chem. Int. Ed.* **2005,** *44* (43), 6996-7023.
18. Shoemaker, D. P.; Hu, Y.-J.; Chung, D. Y.; Halder, G. J.; Chupas, P. J.; Soderholm, L.; Mitchell, J.; Kanatzidis, M. G., In situ studies of a platform for metastable inorganic crystal growth and materials discovery. *Proc. Natl. Acad. Sci. U.S.A.* **2014,** *111* (30), 10922-10927.
19. Scheel, H., Crystallization of sulfides from alkali polysulfide fluxes. *J. Cryst. Growth* **1974,** *24*, 669-673.
20. Axtell, E. A.; Liao, J. H.; Pikramenou, Z.; Kanatzidis, M. G., Dimensional reduction in II-VI materials: $A_2Cd_3Q_4$ (*A* = K, *Q* = S, Se, Te; A= Rb, *Q* = S, Se), novel ternary low-dimensional cadmium chalcogenides produced by incorporation of A_2Q in Cd*Q*. *Chem. Eur. J.* **1996,** *2* (6), 656-666.
21. Huang, F. Q.; Ibers, J. A., New layered materials: Syntheses, structures, and optical properties of $K_2TiCu_2S_4$, $Rb_2TiCu_2S_4$, $Rb_2TiAg_2S_4$, $Cs_2TiAg_2S_4$, and $Cs_2TiCu_2Se_4$. *Inorg. Chem.* **2001,** *40* (11), 2602-2607.
22. Hess, R. F.; Abney, K. D.; Burris, J. L.; Hochheimer, H. D.; Dorhout, P. K., Synthesis and characterization of six new quaternary actinide thiophosphate compounds: $Cs_8U_5(P_3S10)_2(PS_4)_6$, $K_{10}Th_3(P_2S_7)_4(PS_4)_2$ and $A_5An(PS_4)_3$ (*A* = K, Rb, Cs; *An* = U, Th). *Inorg. Chem.* **2001,** *40* (12), 2851-2859.
23. Chen, H.; Rodrigues, J. N.; Rettie, A. J.; Song, T.-B.; Chica, D. G.; Su, X.; Bao, J.-K.; Chung, D. Y.; Kwok, W.-K.; Wagner, L. K., High Hole Mobility and Nonsaturating Giant Magnetoresistance in the New 2D Metal $NaCu_4Se_4$ Synthesized by a Unique Pathway. *J. Am. Chem. Soc.* **2018,** *141* (1), 635-642.
24. Kanatzidis, M. G., Discovery-Synthesis, Design, and Prediction of Chalcogenide Phases. *Inorg. Chem.* **2017,** *56* (6), 3158-3173.
25. Pell, M. A.; Ibers, J. A., Layered ternary and quaternary metal chalcogenides. *Chem. Ber.* **1997,** *130* (1), 1-8.
26. Sangster, J. M., KP (Potassium-Phosphorus) System. *J. Phase Equilib. Diff.* **2010,** *31* (1), 68-72.
27. Tentschev, K.; Gmelin, E.; Hönle, W., Phase transitions crystalline to plastic-crystalline and the specific heat of M_3P_7 compounds (*M* = Li, Na, K, Rb, Cs). *Thermochim. Acta* **1985,** *85*, 151-154.
28. Savelsberg, G.; Schäfer, H., On the Preparation and Crystal Structure of K_3Cu_3P. *Z. Naturforsch. B* **1978,** *33* (6), 590-592.
29. Hönle, W.; Schnering, H. G. V.; Murphy, D., Trisodium Heptaphosphide and Trisodium Undecaphosphide. *Inorganic Syntheses: Nonmolecular Solids* **1995,** *30*, 56-63.
30. Sheldrick, G. M., A short history of SHELX. *Acta Crystallogr. Sect. A: Found. Crystallogr.* **2008,** *64* (1), 112-122.
31. Dolomanov, O. V.; Bourhis, L. J.; Gildea, R. J.; Howard, J. A. K.; Puschmann, H., OLEX2: a complete structure solution, refinement and analysis program. *J. Appl. Crystallogr.* **2009,** *42* (2), 339-341.
32. Petříček, V.; Dušek, M.; Palatinus, L., Crystallographic computing system JANA2006: general features. *Z. Kristallogr. - Cryst. Mater.* **2014,** *229* (5), 345-352.
33. Toby, B. H.; Von Dreele, R. B., GSAS-II: the genesis of a modern open-source all purpose crystallography software package. *J. Appl. Crystallogr.* **2013,** *46* (2), 544-549.
34. Blaha, P.; Schwarz, K.; Madsen, G.; Kvasnicka, D.; Luitz, J., *An augmented plane wave plus local orbital program for calculating crystal properties*. Vienna University of Technology: Vienna, Austria, 2001.
35. Sjöstedt, E.; Nordström, L.; Singh, D., An alternative way of linearizing the augmented plane-wave method. *Solid State Comm.* **2000,** *114* (1), 15-20.
36. Perdew, J. P.; Burke, K.; Ernzerhof, M., Generalized gradient approximation made simple. *Phys. Rev. Lett.* **1996,** *77* (18), 3865-3868.
37. Madsen, G. K.; Singh, D. J., BoltzTraP. A code for calculating band-structure dependent quantities. *Comput. Phys. Commun.* **2006,** *175* (1), 67-71.
38. Blundell, S., *Magnetism in Condensed Matter*. Oxford University Press: New York, 2003.
39. Klapper, H.; Hahn, T., Point-group symmetry and physical properties of crystals. In *International Tables for Crystallography*, 2006; Vol. A, pp 804-808.
40. Wolff, A.; Doert, T.; Hunger, J.; Kaiser, M.; Pallmann, J.; Reinhold, R.; Yogendra, S.; Giebeler, L.; Sichelschmidt, J.; Schnelle, W.; Whiteside, R.; Gunaratne, H. Q. N.; Nockemann, P.; Weigand, J. J.; Brunner, E.; Ruck, M., Low-Temperature Tailoring of Copper-Deficient $Cu_{3-x}P$—Electric Properties, Phase Transitions, and Performance in Lithium-Ion Batteries. *Chem. Mater.* **2018,** *30* (20), 7111-7123.
41. Rettie, A. J.; Sturza, M.; Malliakas, C. D.; Botana, A. S.; Chung, D. Y.; Kanatzidis, M. G., Copper Vacancies and Heavy Holes in the Two-Dimensional Semiconductor $KCu_{3-x}Se_2$. *Chem. Mater.* **2017,** *29* (14), 6114-6121.
42. Sturza, M.; Bugaris, D. E.; Malliakas, C. D.; Han, F.; Chung, D. Y.; Kanatzidis, M. G., Mixed-valent $NaCu_4Se_3$: a two-dimensional metal. *Inorg. Chem.* **2016,** *55* (10), 4884-4890.
43. Olofsson, O., The crystal structure of Cu_3P. *Acta Chem Scand* **1972,** *26* (7), 2777-2787.
44. Hadjiev, V.; Lv, B.; Chu, C., Electronic band structure of $SrCu_4As_2$ and KCu_4As_2: Metals with diversely doped CuAs layers. *Phys. Rev. B* **2011,** *84* (7), 073105.
45. Owens-Baird, B.; Lee, S.; Kovnir, K., Two-dimensional metal $NaCu_{6.3}Sb_3$ and solid-state transformations of sodium copper antimonides. *Dalton Trans.* **2017,** *46* (37), 12438-12445.
46. Sturza, M.; Malliakas, C. D.; Bugaris, D. E.; Han, F.; Chung, D. Y.; Kanatzidis, M. G., $NaCu_6Se_4$: A Layered Compound with Mixed Valency and Metallic Properties. *Inorg. Chem.* **2014,** *53* (22), 12191-12198.
47. Look, D. C., *Electrical characterization of GaAs materials and devices*. Wiley: 1989.
48. Burkov, A.; Heinrich, A.; Vedernikov, M. In *Anisotropic thermoelectric materials, properties and applications*, AIP Conf. Proc, AIP: 1994; pp 76-80.

49. Zeuner, S.; Prettl, W.; Lengfellner, H., Fast thermoelectric response of normal state $YBa_2Cu_3O_{7-\delta}$ films. *Appl. Phys. Lett.* **1995,** *66* (14), 1833-1835.
50. Puggioni, D.; Rondinelli, J. M., Designing a robustly metallic noncenstrosymmetric ruthenate oxide with large thermopower anisotropy. *Nat. Commun.* **2014,** *5* (3432), 1-9.
51. Juza, R.; Bär, K., Conductors and semiconductors among the phosphides of the first and second subgroups. *Z. Anorg Allg. Chem.* **1956,** *283* (1-6), 230-245.
52. Robertson, D.; Snowball, G.; Webber, H., The preparation and properties of single crystal copper phosphide. *J. Mater. Sci.* **1980,** *15* (1), 256-258.

TOC Graphic

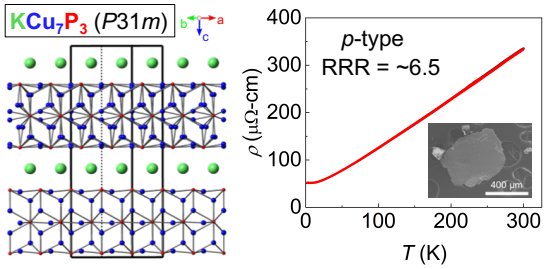

Synopsis: A new, layered copper pnictide, KCu_7P_3 is reported. Geometric displacements of the Cu ions result in a non-centrosymmetic crystal structure. Structural arguments and magnetic measurements show that KCu_7P_3 can be thought of as a dimensionally-reduced derivative of the binary copper phosphide, Cu_3P intercalated with K^+ ions. Combined charge transport measurements and band structure calculations assign KCu_7P_3 as a noncentrosymmetric metal.